Protonated Ozone: Structure, Energetics, and Nonadiabatic Effects

Michele Ceotto,[†] Franco A. Gianturco,*[,†] and David M. Hirst[‡]

Department of Chemistry, The University of Rome, Cittá Universitaria, 00185 Rome, Italy, and Department of Chemistry, Warwick University, Warwick CV47AL, U.K.

Received: July 14, 1999; In Final Form: September 22, 1999

Fully correlated calculations using a multiconfiguration-self-consistent-field (MCSCF) treatment have been carried out to find the most stable structures of $[O_3H]^+$ and to improve on earlier calculations on the same system. The results are used to evaluate proton affinity (PA) and gas-phase basicity of the ozone molecule, quantities which can be compared with experimental data. The existence of regions of nonadiabatic coupling and of charge-exchange effects is evidenced and analyzed, with avoided crossings specifically located for one of the four most stable protonated adducts of ozone. The present study extends the level of accuracy achieved in earlier calculations on the possible structures for protonated ozone and gives specific suggestions on the microscopic processes for the formation of $[O_3H]^+$ in the gas phase.

1. Introduction

The existence of protonated ozone, $[O_3H]^+$, has for many years attracted the interest of experimental and theoretical studies because of its relevance both in gas-phase organic reactions and in photophysically initiated processes in the interstellar medium. For example, the possible existence of neutral and ionic intermediates, O_3H and O_3H^+, has been postulated[1−3] for the nightime production of $O_2(^1\Delta_g)$ in the upper atmosphere, while photodissociated ozone is considered the initiator of the daytime production of that excited oxygen state.[3]

The O_3H^+ ion has been assumed to be an active species when ozone is used for the oxygenation of alkenes in an acid medium,[4−5] while the O_3H^- ion has been postulated[6] as a possible intermediate in the reaction of O_3 with BuO_2H.

In general, the positive ionic species has been the most studied of the above complexes since several experiments indicate its existence as a reactive intermediate in the acid-catalyzed ozonolysis of alkanes[4] and the protonated species can be considered the conjugate acid of one of the least basic simple molecules.[7] There have been various attempts to isolate and characterize such an elusive and important species: Cacace and Speranza,[8,9] for instance, have detected the ion via a mass spectrometric experiment that used the Fourier transform ion cyclotron resonance technique and suggested a proton affinity (PA) value of 148 ± 3 kcal mol^{-1} at 298 K in the gas phase. These authors have also further analyzed the relative basicity order of O_3 with respect to CO and COS,[10] and found $[O_3H]^+$ to be more stable than COH^+ but less stable than $COSH^+$, an interesting ordering in the gas phase that is at odds with other experiments in the condensed phase,[11] where that order was reversed. From a computational point of view the protonated energetics have been the subject of several studies and the calculated PA values range from 124 to 157 kcal mol^{-1} depending on the level of sophistication employed in the calculations,[12−14] which varied from the HF level to correlated CI studies and to DFT models. No consensus seems to have been reached, however, on the actual energy values nor on the most likely geometries that can be associated with protonated ozone in its ground electronic state. Furthermore, the energy difference between the O_3 ionization potential (12.53 eV) and that of H suggests that the protonated adduct can dissociate either via a charge-transfer (CT) channel or via an electron-transfer (ET) channel, the latter being more favorable by 1.07 eV:

$$\begin{aligned}(O_3H)^+ &\rightarrow O_3 + H^+(CT)\\ &\rightarrow O_3^+ + H(ET)\end{aligned} \qquad (1)$$

thereby indicating that nonadiabatic effects are bound to be present between the relevant, multidimensional, Born−Oppenheimer (BO) potential energy surfaces and that their location within the molecular geometry phase space constitutes both an interesting aspect of the theoretical analysis and a physical mechanism likely to be involved in forming the protonated molecule. One should keep in mind, in fact, that regions of avoided crossings in one dimension can give rise to conical intersections in many dimensions and have been found to occur during the dynamics of molecular protonation in the gas phase.[7,15,16]

In the present study we are therefore revisiting the structures of the $[O_3H]^+$ species by carrying out calculations at a more advanced level of correlation corrections than done before and by further analyzing the following aspects of the problem: (i) accurate determination of PA and gas-phase basicity by full optimization of the structures and by analysis of the basis set consistency problems; (ii) discussion of the asymptotic states, location of the regions of nonadiabatic effects, and assessment of their importance during protonation dynamics; (iii) a more realistic comparison with experimental data by explicit inclusion of temperature effects and entropic corrections for the final energetics.

The following section briefly describes the computational methods, while section 3 reports our search for the optimal structures of the bound protonated ozone species and the different electronuclear contributions to their binding energies. Sections 4 and 5 describe the detailed evaluation of the gas-phase basicity and the location of the nonadiabatic coupling

* Corresponding author. E-mail: fagiant@Caspur.it.
[†] The University of Rome.
[‡] Warwick University.

10.1021/jp9923769 CCC: $18.00
Published on Web 11/12/1999

region along either the proton approach or the dissociative pathways. The conclusions of the present study are summarized in section 6.

2. The Theoretical Method

As mentioned before, the first ab initio calculations for the $[O_3H]^+$ species were done[12] at the SCF level and attempted to approach the Hartree−Fock (HF) limit by using first an STO-3G basis set and then a slightly larger 4-31G basis set. Later calculations[13] on the same system used first the SCF level of computation by employing a (DZ+P) Gaussian basis set and then improved it by performing coupled-cluster (CC) correlation calculations which included all single and double substitutions, the CCSD formalism.[18] By further using analytic gradient methods via simple harmonic frequencies from SCF second derivatives, Schaefer et al. obtained[19] more precise locations for the four lowest stable structures of the adduct.

In the present analysis we decided to extend the above studies one step further by generating larger regions of the relevant potential energy surfaces (PES) and by analyzing in greater detail the effects of both basis set consistency and correlation corrections.

We started with a double-ζ-plus-polarization (DZ+P) basis set of GTOs and the relevant molecular orbitals were obtained using the second-order direct multiconfiguration method of Werner and Knowles,[20,21] as available in the MOLPRO suite of programs.

The orbital space was therefore divided into an internal space (IS) with 10 orbitals. The IS subspace was further partitioned into three different regions: (i) the core orbitals (COs) which are doubly occupied but kept frozen and uncorrelated during the CI process; (ii) the closed-shell orbitals (CSOs) which are also doubly occupied but included in the correlation process, and (iii) the active orbitals (AOs) which are employed to define the active space for the CI procedure. As is well-known, such partitioning improves the speed of computational performance and brings its level of correlation corrections to that of a complete-active-space SCF (CASSCF) using an active space equal to our entire IS.[22] We therefore carried out calculations at two different levels: we first kept the three oxygen (1s) orbitals frozen and defined them as our COs during the multiconfigurational calculations (this will be called the MC-SCF-core type of calculation) and then we relaxed this constraint by promoting the (1s) orbitals to the level of correlation of our CSO subspace with the AO subspace. We shall call such calculations the MCSCF-close type of calculation.

We further extended our (DZ+P) results by carrying out exactly the same types of calculations at the valence-plus-triple-ζ (VTZ) level and further up to very large (VQZ and V5Z) expansions.[22] The convergence achieved by our final PA values will then be examined in the last section of the present paper.

3. Optimized Protonated Adducts

As briefly mentioned above, several computational studies have been carried out in the past on the possible structures for the protonated ozone molecule in its ground electronic state and in the gas phase. The earliest calculations were by Kausch and Schleyer,[12] who optimized the geometric structures of four possible arrangements by using a minimal STO-3G basis and then reoptimized the final geometries using a 4-31G basis set with second-order Möller−Plesset perturbation (MP2) at both the 4-31G and the 6-31G levels of expansion. The above calculations were followed shortly after by the SCF study of Mathisen, Gropen, Skancke, and Wahlgren,[3] who used both

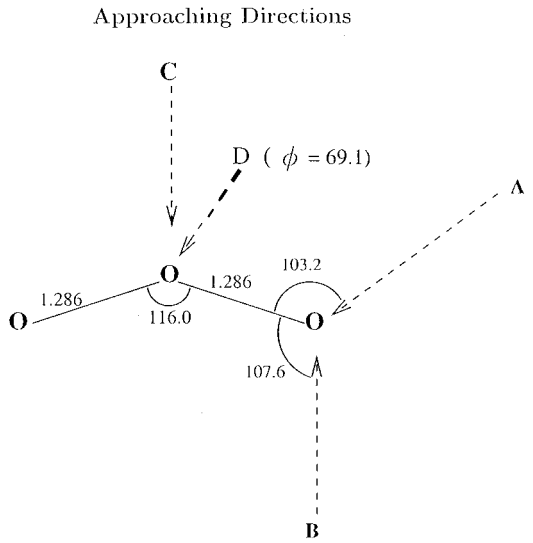

Figure 1. Geometrical configurations of the four cuts of the full potential energy surface examined in the present work. The numbering from A to D is the one followed in the main text. Distance in Å and angles in degrees.

medium (double-ζ) basis sets and larger basis sets as described in their work.[3] That study attempted to determine the structure of $(O_3H)^+$ as well as address the question of whether the protonation might preferentially stabilize cyclic ozone enough to make it competitive with the open forms, while reference 5 tried to obtain relative stability data by using (at the SCF level) increasingly larger basis set expansions. Their findings were largely consistent with those of Kausch and Schleyer.[12]

Additional calculations on the possible structures of the protonated adduct were carried out more recently by Meredith, Quelch, and Schaefer,[13] who specifically wanted to investigate the relative probabilities of obtaining protonation of the open-chain (C_{2v}) and cyclic (D_{3h}) forms since their earlier calculations[23] indicated that the electron correlation contributions are more important for the C_{2v} isomer than for the D_{3h} form of isolated ozone. They applied methods more sophisticated than before to handle the correlation corrections by using coupled-cluster theory with single and double substitutions (CCSD) and an extended basis set to the double-ζ-plus-polarization (DZ+P) type that reproduced very well the experimental equilibrium geometry and the harmonic vibrational frequencies of the isolated molecule. They performed geometry optimization by using SCF and CCSD analytic gradient methods and isolated four specific structures as the most stable. We shall call such structures the A, B, C, and D forms: they are pictorially summarized in Figure 1. The structure labeled as the D form corresponds to the H^+ partner coming onto the central oxygen atom from above the plane of the ozone molecule, at the angle with that plane reported in the figure (69.1°).[13]

It is well-known that ozone is difficult to discuss theoretically due to its diradical character, shown fairly clearly by the spatial shape of its $1a_2$ molecular orbital (MO) which is nearly exclusively located on the two wing atoms, and by the existence of an equally important configuration when the $1b_1$ orbital is occupied instead[13] (see below). The correlation contributions by the different dominant configurations, therefore, greatly affect the relative stability and sequential energetics of the various protonated species. The results of ref 13 indicated that protonation preferentially stabilizes the open-chain form (configuration A) with respect to the ring form (configuration D) and found a ΔE (chain-ring) energy difference of 23.2 kcal/mol^{-1}.

TABLE 1: Geometry of Isolated Ozone Molecule (X^1A_1)

	optimized geometries from present work			calculations using MRD-CI geometries (from ref 24)		
	SCF	MCSCF (core)	MCSCF (close)	SCF	MCSCF (core)	MCSCF (close)
R_1 (Å)	1.207	1.262	1.264	1.286	1.286	1.286
R_2 (Å)	1.207	1.262	1.264	1.286	1.286	1.286
θ (deg)	118.9	117.1	117.0	116.0	116.0	116.0
E_{TOT} (au)	−224.320 90	−224.473 83	−224.475 78	−224.304 03	−224.472 62	−224.474 85

TABLE 2: Optimized Geometries of the Protonated Moiety (see Figure 1)

	protonated ozone at geometry A			protonated ozone at geometry B		
	SCF	MCSCF (core)	MCSCF (close)	SCF	MCSCF (core)	MCSCF (close)
R_1 (Å)	1.144	1.182	1.196	1.147	1.188	1.206
R_2 (Å)	1.343	1.611	1.466	1.331	1.609	1.437
θ_1 (deg)	112.9	112.9	113.5	118.1	118.4	117.6
θ_2 (deg)	103.0	97.7	99.8	107.3	103.0	104.4
$R_{O_3-H^+}$ (Å)	0.975	1.003	1.007	0.978	1.006	1.012
E_{TOT} (au)	−224.580 387	−224.779 26	−224.812 07	−224.573 01	−224.773 45	−224.807 27
PE_{AD} (au)	−0.2594 87	−0.3054 37	−0.3362 89	−0.252 11	−0.299 62	−0.331 49
PE_{AD} (kcal/mol)	−162.83	−191.66	−211.02	−158.20	−188.01	−208.01
	protonated ozone at geometry C			protonated ozone at geometry D		
	SCF	MCSCF (core)	MCSCF (close)	SCF	MCSCF (core)	MCSCF (close)
R_1 (Å)	1.212	1.332	1.315	1.391	1.508	1.485
R_2 (Å)	1.212	1.332	1.315	1.391	1.508	1.485
θ_1 (deg)	127.0	123.5	124.3	58.4	60.3	60.2
θ_2 (deg)	116.5	118.25	117.9	69.4	77.5	74.8
$R_{O_3-H^+}$ (Å)	1.015	0.990	0.996	0.989	1.003	1.019
E_{TOT} (au)	−224.451 743	−224.689 023	−224.717 739	−224.509 164	−224.703 415	−224.737 777
PE_{AD} (au)	−0.130 843	−0.215 193	−0.241 959	−0.188 264	−0.229 315	−0.261 997
PE_{AD} (kcal/mol)	−82.11	−135.04	−151.83	−118.14	−143.90	−164.41

This behavior is chiefly due to the partial destruction of the O_3 diradical character by protonation on the terminal oxygen of the C_{2v} geometry, whereby the addition of the H^+ on a terminal, negatively charged atom tends to localize the charge on that end of the molecule so that the entire electronic structure is frozen into one of the two nearly degenerate dominant structures of the isolated ozone.[13]

A more empirical approach was employed in a further set of calculations[14] where the authors used a linear combination of Gaussian orbitals with density functional models (LCGTO-DF) and employed local and nonlocal exchange-correlation functionals. Their results were essentially in agreement with those of Meredith et al.,[13] although the differences in the method employed yielded energy spacings which were only in qualitative agreement with the previous findings.

Our results shown in Table 1, where the various levels of optimization for the isolated molecule O_3 are presented, allow us to draw the following conclusions:

(i) As expected, the SCF results give shorter bonds and show greater repulsion between wing atom charges.

(ii) The increased correlation afforded by the MCSCF-close results is seen by the marked energy lowering since the geometries change very little from those of the MCSCF-core calculations.

(iii) When we employed the geometries produced by the earlier MRD-CI calculations which expanded the wave function on a larger basis set, we obtained a total energy slightly higher than their value (which was −225.026 64 au) but also found that the present optimization procedure with our higher level of correlation can cause variations in the final structure, in both bond length and bond angle values.

Since the above results indicate that the level of correlation we included when treating the O_3 target ground electronic state is capable of describing that molecule very closely to the results from the best available calculations on it,[14] we proceeded to analyze the approaching pathways of the proton along the orientations suggested by the earlier work[13] and selected in Figure 1. We carried out the evaluation of the selective "cuts" of the lowest potential energy surface (PES) in the region of the protonated adduct by using first the O_3 geometry given by ref 24. Since the ozone ionization potential, as mentioned before, is slightly lower than the H ionization energy by about 1 eV, the protonated moiety can adiabatically dissociate into the $O_3^+ + H$ channel as its lowest energetic channel but can also undergo, on its way to full dissociation, nonadiabatic coupling with the next asymptotic channel associated to the $O_3 + H^+$ system: our present study has focused on the two lowest PES and on their minimum energy regions along the four pathways suggested by the geometries of Figure 1. The presence of the $O_3^+ + H$ asymptotic channel has been controlled during dissociation by evaluating the ozone charge obtained from the wave function associated to that energy root: it was always found to be given as +1.

The marked effect of correlation energy, and of correlation energy changes in going from O_3 to its protonated species could be seen from the results reported in Table 2. The approach of the proton is carried out by keeping the O_3 frozen at its best optimized geometry as given in the last two columns of Table 1. That this is a realistic choice could be concluded from our further calculations, where all the protonated forms were studied around their equilibrium minima by carrying out two different computations: we first evaluated the total energies of the lowest electronic states around the minima position of the $R_{O_3-H^+}$ coordinate with the O_3 geometry "frozen" to its isolated optimal value (as given by ref 24). We then repeated the calculations by optimizing the geometry of the ozone partner within each adduct at each relative configuration. We clearly saw that the minimum energy positions of the added atom is not significantly altered by the global optimization, while the total energy values can still change by several millietectronvolts. This point will

TABLE 3: Counterpoise Corrections for Two of the Protonated Structures (A and B Configurations from Figure 1; All Quantities in mhartrees)

	calculations done at geometry A			calculations done at geometry B		
$R_{O_3-H^+}$ (Å)	SCF	MCSCF (core)	MCSCF (close)	SCF	MCSCF (core)	MCSCF (close)
0.4	2.78	35.17	68.25	3.14	35.55	68.63
0.7	2.06	34.50	67.57	2.56	35.03	68.12
1.0	1.51	33.94	67.00	2.06	34.52	67.60
1.3	1.07	33.49	66.53	1.57	34.04	67.11
1.6	0.82	33.28	66.31	1.27	33.75	66.80
1.9	0.64	33.11	66.15	0.99	33.49	66.53
2.2	0.44	32.93	65.95	0.72	33.23	66.25
2.5	0.29	32.79	65.81	0.52	33.04	66.06
2.8	0.21	32.71	65.72	0.38	32.90	65.92
3.1	0.14	32.65	65.66	0.26	32.79	65.80
3.4	0.09	32.61	65.61	0.17	32.68	65.69
3.7	0.05	32.58	65.57	0.09	32.62	65.61
4.0	0.03	32.55	65.54	0.05	32.58	65.57

therefore be important when we will later evaluate the gas-phase basicity of the species but tells us that, as expected, the optimized structures are reached with negligible intermolecular correlation effects for the protonated process.

In Table 2 we report the final, fully optimized, geometries of the four stable forms of the protonated species. In agreement with what was shown by the best of the previous computational estimates,[13] our results indicate that the protonation of ozone can occur both in the open-chain and in other configurations, whereby the approaching H^+ binds either to one of the wing oxygens or to the central one. However, its most stable form is provided by the open chain of configuration A of Figure 1. It is also interesting to note the following:

(i) The inclusion of inner-electron correlation afforded by the MCSCF-close calculations is clearly an important correction for a better estimate of correlation effects.

(ii) Bond distances are markedly shortened by the presence of the additional charge as intramolecular polarization and charge-transfer effects reduce nuclear shielding within the O_3 partner.

(iii) The same effect of above is also seen in the reduction of the bond angle within ozone in the A, D, and C forms and in an *increase* of that angle for the B form.

(iv) The bound proton is located nearer the wing oxygen atom, at distances which are shorter than both R_{O-O} bonds.

As a preliminary indicator, we also show in Table 2 the values of the adiabatic protonation energy (PE) obtained by simple energy differences between the optimized configuration of O_3H^+ and that of isolated O_3, i.e., by allowing the O_3 geometry to relax into the minimum configuration of the adduct when coming from the isolated O_3. The values of the protonation energies given by this approach are larger than those produced when including the further corrections that we will be discussing in the following section. However, we already see from the analysis of the four most stable structures that the corresponding PE values vary markedly from each other, spanning a fairly broad band of energies.

First the effects of the basis set superposition errors (BSSE) in the evaluation of the energy differences between protonated species and asymptotic fragments should be considered. Briefly, the supermolecular picture we are employing here defines the interaction energy of a complex MA as given by the difference

$$\Delta E(R) = E_{MA}(R) - E_M - E_A \qquad (2)$$

where R is the reaction coordinate and the internal geometry of M, for the time being, is not supposed to change during the separation between partners. One usually assumes in the above equation that for large separations E_{MA} reduces to the sum of $E_M + E_A$ and the latter contributions are assumed to be evaluated using the M basis set for the former and the A basis set for the latter. However, it is now well-recognized[25] that the results one may obtain for ΔE in this way are too negative because, as R decreases, not only is the interaction switched on but also the monomers present in MA can start using the one-electron basis set of each partner in the complex, thereby providing an additional stabilization which has nothing to do with the correct energy difference.

This type of error can be avoided by calculating the interaction energy via the counterpoise (CP) function correction introduced by Boys and Bernardi[28]

$$\Delta E^{CP}(R) = E_{MA}(R) - E_M^{(MA)}(R) - E_A^{(MA)}(R) \qquad (3)$$

where E_M(MA) and E_A(MA) are now the partner energies obtained by using the full adduct basis at the particular R geometry one is considering. The matching error, usually termed the BSSE error, can be obtained as

$$\mathrm{BSSE} = E_M^{(MA)}(R) + E_A^{(MA)}(R) - E_M - E_A \qquad (4)$$

The same quantity is also often termed the orbital basis inconsistency (OBI) error.[29] One should keep in mind that, for very large interpartner separations, the BSSE error has to go to zero but the CP correction does not. This is because the latter procedure also corrects for size consistency errors (SCE) in the basis set choice. Thus, what is shown by the CP results combines both corrections. Furthermore, for very extended basis set choices the basis saturation effects cause the BSSE correction to become rather negligible, as we shall further see from our results below.

Our calculations are reported in Table 3 for two of the open-chain forms of the protonated adducts which we have discussed before. To match the definition implicit in eq 3, we have kept the O_3 geometry at its "frozen" value already obtained from the full CI results for the O_3H^+ given by Table 2.

The results of the table indicate the energy corrections to the O_3 ground state electronic energy when the full basis set of the O_3H^+ species is employed for the proton approach along the coordinates of the A (third and fourth columns) and the B (sixth and seventh column) forms, respectively. One clearly sees that for both forms the CP correction is exactly of the same value and that it is fairly constant along R. On the other hand, we also see that at the MC level the correlation corrections play a rather evident role: the results show the CP correction both when the MC procedure was carried out at the MCSCF-core

TABLE 4: Calculated Contributions to the O_3H^+ Proton Affinity (PA) for the Open-Chain Form A of Figure 1

	fixed nuclei			adiabatic		
	SCF	MCSCF (core)	MCSCF (close)	SCF	MCSCF (core)	MCSCF (close)
$E_{TOT}(O_3)$ (au)	−224.304 035[a]	−224.472 623[a]	−224.474 851[a]	−224.320 90[b]	−224.473 83[b]	−224.475 78[b]
CP correction (au, kcal/mol)[d]	0.001 502 4, +0.94	0.033 938 9, +21.30	0.066 996 8, +42.04	0.001 502 4, +0.94	0.033 938 9, +21.30	0.066 996 8, +42.04
$R_{O_3-H^+}$ (Å)	0.9776	0.9983	1.0078	0.975	1.003	1.007
$E_{TOT}(O_3H^+)$ (au)	−224.549 066	−224.758 857	−224.799 736	−224.580 39	−224.779 26	−224.812 07
CP corrected protonation energy (PE) (au, kcal/mol)	−0.243 528 6, −152.82	−0.252 295 1, −158.31	−0.257 888 2, −161.83	−0.25 798 46, −161.88	−0.271 498 1, −170.37	−0.269 292 2, −168.98
$(5/2)RT$[c] (kcal/mol)	+1.48	+1.48	+1.48	+1.48	+1.48	+1.48
$\partial^2E/\partial R_{O_3-H^+}{}^2$ [e] (hartree/bohr^2)	1.863 287	1.457 404	1.507 481	2.314 705	2.207 273	2.186 970
$[E_{vib}(O_3H^+) - E_{vib}(O_3)]$ (kcal/mol)	+1.61	+1.43	+1.45	+1.80	+1.76	+1.75
$-\Delta H$ (kcal/mol) = PA	149.73	155.40	158.90	158.61	167.13	165.75

[a] Ozone partner at the full CI geometry of Table 1. [b] Optimized ozone partner geometries as obtained in present work. [c] $(5/2)RT = \Delta(PV) + (3/2)RT$. [d] From the PES cuts of Figure 2. [e] From the Hessian of the PES (see main text).

level and also when the core electrons were included in the MCSCF-close calculations. In the latter case, therefore, to employ a more extended one-electron basis within the MC procedure yields a OBI error, hence a CP correction, which is nearly twice as big as in the previous case. The values vary between 20 and 42 kcal/mol and clearly suggest that the previous estimates of the PE values shown in Table 2 constituted only preliminary data, as we shall discuss with more detail in the following section. The final CP correction used below for the protonated adducts was that obtained at the O_3H^+ distance of 1 Å. One should note that, in the case of a supermolecular calculation near the equilibrium structure of the adduct, the CP correction is really chiefly giving us the BSSE correction as the OBI contribution plays there a minor role.

4. Evaluation of Gas-Phase Basicity

To be able to compare computed values with existing, or future, experimental data, one has to clearly and carefully define the various quantities which, both experimentally and theoretically, can play a role in the protonation process.

In terms of macroscopic quantities which relate to the equilibrium situation in the gas phase, one evaluates the gas basicity (GB) of the process

$$O_3(\text{gas}) + H^+(\text{gas}) \rightarrow O_3H^+(\text{gas}) \qquad (5)$$

and defines it as the negative of the standard Gibbs energy variation $\Delta G = \Delta H - T\Delta S$. Hence one can obtain the proton affinity (PA) as the negative of the enthalpy change[14]

$$\text{PA} = -\Delta H = -\Delta U - \Delta(PV) = -\Delta E - [E_{int}(O_3H^+) - E_{int}(O_3)] - (5/2)RT \qquad (6)$$

where $(5/2)RT$ is the sum of $\Delta(PV)$ and the difference in the proton translational contributions to the internal energy, in the gas phase, at the temperature T of process 6. In the present case, however, this difference is chiefly due to the proton translation energy when free from the adduct. The crucial quantity is therefore the computed protonation energy (PE) given as the first term on the right-hand side of eq 6:

$$\text{PE}_{AD} = \Delta E = E^{AD}{}_{O_3H^+} - E^{AD}{}_{O_3} \qquad (7)$$

$$\text{PE}_{FN} = \Delta E = E^{FN}_{O_3H^+} - E^{FN}_{O_3} \qquad (8)$$

where $E_{O_3H^+}$ and E_{O_3} indicate ab initio calculations obtained within the BO approximation, either within the fixed-nuclei (FN) scheme for the initial and final internal structures of ozone of eq 6 or by relaxing the molecular structure within the final adduct (AD results).

The second contribution shown on the right-hand side of eq 6, and given within square brackets, describes the difference in internal energy content between the isolated partner and its protonated adduct at the temperature for which process 5 is carried out. This is obviously a more difficult quantity to evaluate as several degrees of freedom are involved. If we consider the changes due to electronic contributions as being already taken into account by the ΔE value of eqs 7 and 8 (both species remain in their ground electronic states) and we further disregard the difference due to rotational contributions (the O_3 asymmetric rotor is only slightly deformed by the presence of the light H^+ bound to it), then we are left with the evaluation of the vibrational energy changes, $\Delta E_{vib}(T)$, that contribute to the term in square brackets of eq 6. The latter quantity can be further simplified by merely considering both species as chiefly populating their ground vibrational states and therefore by estimating a temperature-independent variation between the zero point energies (ZPEs) of the two species. Hence, one can obtain from the Hessian of the PES in each of the forms of Figure 1 an estimate of the energy second derivative that can give us the corresponding force constant within the harmonic approximation. This last quantity will therefore be our calculated ΔE_{ZPE} for process 5.

Finally, we further need to evaluate the entropy variation as

$$-T\Delta S = -T[S(O_3H^+) - S(O_3) - S(H^+)] \qquad (9)$$

which we decided to evaluate explicitly by considering all the entropy contributions for each of the four possible structures of the adducts.[30]

We show in Tables 4−7 the results associated with the four most stable conformations of the protonated moieties from A to D. All the contributions discussed before have been included, and the origins of their values are briefly indicated in the footnotes of the tables. We also report there for comparison the results obtained using both the FN and the AD approaches.

One clearly sees there the following points:

(i) The correlation correction, as already seen in Table 2, hardly changes the value of the proton position at the energy minimum, and the same occurs when full O_3 relaxation of geometry is included.

(ii) The adiabatic PE values obtained now are markedly smaller than the ones qualitatively discussed for our calculations

TABLE 5: Calculated Contributions to the O_3H^+ Proton Affinity (PA) for the Open-Chain Form B of Figure 1

	fixed nuclei			adiabatic		
	SCF	MCSCF (core)	MCSCF (close)	SCF	MCSCF (core)	MCSCF (close)
$E_{TOT}(O_3)$ (au)	−224.304 035[a]	−224.472 623[a]	−224.474 851[a]	−224.320 90[b]	−224.473 83[b]	−224.475 78[b]
CP correction (au, kcal/mol)[d]	0.002 059 6, +1.29	0.034 522 2, +21.66	0.067 600 9, +42.42	0.002 059 6, +1.29	0.034 522 2, +21.66	0.067 600 9, +42.42
$R_{O_3-H^+}$ (Å)	0.9792	1.0021	1.0139	0.9782	1.0065	1.0017
$E_{TOT}(O_3H^+)$ (au)	−224.544 453	−224.757 589	−224.798 023	−224.573 007	−224.773 455	−224.807 269
CP corrected protonation energy (PE) (au, kcal/mol)	−0.238 358 4, −159.57	−0.250 443 8, −157.16	−0.255 571 1, −160.37	−0.250 0947 4, −156.91	−0.265 102 8, −166.35	−0.263 888 1, −165.59
(5/2)RT[c] (kcal/mol)	+1.48	+1.48	+1.48	+1.48	+1.48	+1.48
$\partial^2E/\partial R_{O_3-H^+}{}^2$ [e] (hartree/bohr^2)	1.833 461	1.419 506	1.407 833	2.358 983	1.738 800	2.174 168
$[E_{vib}(O_3H^+) - E_{vib}(O_3)]$ (kcal/mol)	+1.60	+1.41	+1.40	+1.82	+1.56	+1.74
$-\Delta H$ (kcal/mol) = PA	146.49	154.27	157.49	153.61	163.32	162.37

[a] Ozone partner at full CI geometry. [b] Optimized ozone partner geometries as obtained in present work. [c] (5/2)$RT = \Delta(PV) + (3/2)RT$. [d] From the PES cuts of Figure 2. [e] From the Hessian of the full PES (see main text).

TABLE 6: Calculated Contributions to the O_3H^+ Proton Affinity (PA) for the Open-Chain Form C of Figure 1

	fixed nuclei			adiabatic		
	SCF	MCSCF (core)	MCSCF (close)	SCF	MCSCF (core)	MCSCF (close)
$E_{TOT}(O_3)$ (au)	−224.304 035[a]	−224.472 623[a]	−224.474 851[a]	−224.320 90[b]	−224.473 83[b]	−224.475 78[b]
CP correction (au, kcal/mol)	−0.240 823 1, −151.12	0.022 748 5, +14.27	0.059 832 1, +37.54	−0.240 823 1, −151.12	0.022 748 5, +14.27	0.059 832 1, +37.54
$R_{O_3-H^+}$ (Å)	1.0130	0.9999	0.9999	1.0155	0.9898	0.9958
$E_{TOT}(O_3H^+)$ (au)	−224.433 259	−224.648 355	−224.650 598	−224.451 743	−224.689 023	−224.717 739
CP corrected protonation energy (PE) (au, kcal/mol)	−0.370 047 1, −232.21	−0.152 983 5, −96.00	−0.115 914 9, −72.74	−0.371 666 1, −233.22	−0.192 444 5, −120.76	−0.182 126 9, −114.29
(5/2)RT[c] (kcal/mol)	+1.48	+1.48	+1.48	+1.48	+1.48	+1.48
$\partial^2E/\partial R_{O_3-H^+}{}^2$ [d] (hartree/bohr^2)	1.392 855	1.541 155	1.538 823	2.225 809	2.828 323	2.311 612
$[E_{vib}(O_3H^+) - E_{vib}(O_3)]$ (kcal/mol)	+1.39	+1.47	+1.47	+1.76	+1.99	+1.80
$-\Delta H$ (kcal/mol) = PA	229.34	92.54	69.79	229.99	117.30	111.01

[a] Ozone partner at full CI geometry. [b] Optimized ozone partner geometries as obtained in present work. [c] (5/2)$RT = \Delta(PV) + (3/2)RT$. [d] From the Hessian of the full PES (see main text).

TABLE 7: Calculated Contributions to the O_3H^+ Proton Affinity (PA) for the Open-Chain Form D of Figure 1

	fixed nuclei			adiabatic		
	SCF	MCSCF (core)	MCSCF (close)	SCF	MCSCF (core)	MCSCF (close)
$E_{TOT}(O_3)$ (au)	−224.304 035[a]	−224.472 623[a]	−224.474 851[a]	−224.320 90[b]	−224.473 83[b]	−224.475 78[b]
CP correction (au, kcal/mol)	−0.194 606 8, −122.12	0.032 082 1, +20.13	0.067 344 6, +42.26	−0.194 606 8, −122.12	0.032 082 1, +20.13	0.067 344 6, +42.26
$R_{O_3-H^+}$ (Å)	1.0354	1.0004	1.0321	0.9891	1.0034	1.0191
$E_{TOT}(O_3H^+)$ (au)	−224.387 166	−224.606 213	−224.691 260	−224.509 164	−224.703 145	−224.737 777
CP corrected protonation energy (PE) (au, kcal/mol)	−0.277 737 8, −174.28	−0.101 507 9, −63.70	−0.149 064 4, −93.54	−0.382 870 8, −240.25	−0.197 232 9, −123.77	−0.194 652 4, −122.15
(5/2)RT[c] (kcal/mol)	+1.48	+1.48	+1.48	+1.48	+1.48	+1.48
$\partial^2E/\partial R_{O_3-H^+}{}^2$ [e] (hartree/bohr^2)	1.211 984	1.551 966	1.283 026	2.370 573	2.274 964	2.281 362
$[E_{vib}(O_3H^+) - E_{vib}(O_3)]$ (kcal/mol)	+1.30	+1.47	+1.34	+1.82	+1.78	+1.79
$-\Delta H$ (kcal/mol) = PA	171.50	60.75	90.72	236.96	120.51	118.88

of Table 2. Hence the CP correction is an essential ingredient when MCSCF calculations for the supermolecule are carried out.

(iii) The ΔE_{ZPE} estimates using the full Hessian of the relevant PES add a significant correction and help to obtain proton affinity (PA) values which can be more directly compared with what has been experimentally measured: they are seen to be here smaller than our previous PE values.

The quantity that our calculations can also produce is the full, observable ΔG value as a measure of the gas basicity (GB) of the molecular target

$$\Delta G = \mathrm{GB} = \mathrm{PA} - T\Delta S \qquad (10)$$

which we report in Table 8 for the four configurations discussed in the present work, using our rigorously calculated entropy contributions for each of the four protonated adducts.[30] We used the vibrational frequency values from ref 13 and followed the equipartition theorem.

The comparison with the experimental value of ref 8 indicates that the two A and B configurations are possibly the more likely candidates for the description of the most stable O_3H^+ geometry as they show larger GB values. Furthermore, all FN computed values, i.e., the ones obtained with the unchanged O_3 geometry in the adduct (GB_{FN}) are smaller than those given by the optimized geometries (GB_{AD}) which remain, however, still larger than the experimental values.[8] The difference which still appears between the latter and the available experiment will be further discussed below.

To make the present comparison more quantitative, we have first extended our analysis to the basis set effects on protonation energy values and report in Tables 9−12 the convergence study for the four different protonated adducts of the present work. We can make the following considerations from a perusal of the results:

(ii) The PE value rapidly converges when the basis set is extended beyond the VTZ level and shows very little change

TABLE 8: Computed and Experimental Values for the Gas Basicity (GB) of the Ozone Molecule[d]

	protonated species							
	A		B		C		D	
	FN	AD	FN	AD	FN	AD	FN	AD
PA (kcal/mol)	158.90	162.12	157.49	162.37	69.79	111.01	90.72	118.88
$T\Delta S$ (kcal/mol)	7.76[a]	6.95[b]	7.76[a]	6.95[b]	7.76[a]	7.22[b]	7.76[a]	7.23[b]
ΔG (kcal/mol)	151.14	155.17	149.73	155.42	62.03	103.79	82.96	111.65
ΔG_{exp} (kcal/mol) = GB_{exp}				140 ± 3[c]				

[a] As estimated with the formula $\Delta S = R \ln[\sigma(O_3)/\sigma(O_3H^+)]$. [b] Theoretical estimates of this work. [c] From ref 8. [d] FN = fixed nuclei calculations; AD = adiabatic calculations.

TABLE 9: Basis Set Optimization Geometry Test and PE for Isolated Ozone and for the Protonated Adduct in Geometry A

	DZP	VTZc	VTZ	VQZc	VQZ	V5Z
R_{O-O} (Å)	1.264	1.282	1.282	1.279	1.279	1.283
θ (deg)	117.0	116.8	116.8	116.9	116.9	116.8
E_{O_3} (au)	−224.475 780	−224.569 003 37	−224.569 692 86	−224.585 929 01	−224.586 085 88	−224.584 096 68
$E_{O_3H^+}$ (au)	−224.812 07	−224.846 214 89	−224.846 914 15	−224.863 410 71	−224.863 578 10	−224.861 571 72
PE_{AD} (kcal/mol)	−211.02	−173.95	−173.96	−174.12	−174.13	−174.12
CP correction (kcal/mol)	+42.04	+0.47	+0.42	+0.16	+0.16	+0.12
PE^{CP} (kcal/mol)	−168.98	−173.48	−173.53	−173.96	−173.97	−174.00

TABLE 10: Basis Set Optimization Geometry Test and PE for Isolated Ozone and for the Protonated Adduct in Geometry B

	DZP	VTZc	VTZ	VQZc	VQZ	V5Z
E_{O_3} (au)	−224.475 780	−224.569 003 37	−224.569 692 86	−224.585 929 01	−224.586 085 88	−224.584 096 68
$E_{O_3H^+}$ (au)	−224.807 270	−224.841 389 47	−224.842 158 42	−224.858 708 44	−224.858 877 23	−224.856 759 99
PE_{AD} (kcal/mol)	−208.01	−170.92	−170.97	−171.17	−171.18	−171.10
CP correction (kcal/mol)	+42.42	+0.78	+0.68	+0.29	+0.29	+0.24
PE^{CP} (kcal/mol)	−165.59	−170.14	−170.29	170.88	170.89	170.86

TABLE 11: Basis Set Test at Fixed Optimized Geometry and PE for Isolated Ozone and for the Protonated Adduct in Geometry C

	DZP	VTZc	VTZ	VQZc	VQZ	V5Z
E_{O_3} (au)	−224.475 780	−224.569 003 37	−224.569 692 86	−224.585 929 01	−224.586 085 88	−224.584 096 68
$E_{O_3H^+}$ (au)	−224.717 739	−224.736 431 04	−224.737 008 26	−224.753 909 51	−224.754 142 36	−224.750 640 67
PE_{AD}[a] (kcal/mol)	−151.83	−105.06	−104.99	−105.41	−105.46	−104.51

[a] Protonation energy (PE) without CP correction.

TABLE 12: Basis Set Test at Fixed Optimized Geometry and PE for Isolated Ozone and for the Protonated Adduct in Geometry D

	DZP	VTZc	VTZ	VQZc	VQZ	V5Z
E_{O_3} (au)	−224.475 780	−224.569 003 37	−224.569 692 86	−224.585 929 01	−224.586 085 88	−224.584 096 68
$E_{O_3H^+}$ (au)	−224.737 777	−224.770 682 71	−224.771 662 24	−224.787 374 77	−224.787 464 85	−224.784 728 78
PE_{AD}[a] (kcal/mol)	−164.41	−126.56	−126.74	−126.41	−126.37	−125.90

[a] Protonation energy (PE) without CP correction.

when the basis set is further enlarged. Furthermore, the final changes from the values with the DZP basis shown in Tables 4−7 are only about 3%.

(ii) The CP corrections, as expected, become increasingly smaller and reveal clearly the basis saturation effects mentioned in the previous discussion.

(iii) All geometries have been optimized within each chosen basis set, for both the adduct and the isolated ozone particle. We therefore see again that protonation changes only negligibly the molecular partner geometry within the adduct.

We also see now that, when the value of the asymptotic energy difference between the ($O_3 + H^+$) and the ($O_3^+ + H$) channel (23.3 kcal/mol) is subtracted from the upper fragmentation pathway (leading to $O_3 + H^+$) in order to obtain the lower fragmentation pathway (leading to $O_3^+ + H$), the experimental value of the PA becomes remarkably well reproduced by the computed, ZPE-corrected, PE value for the most stable adduct given in Table 9: the computed PA becomes in fact (see also Table 4) 147.5 kcal/mol, to be compared with the experimental estimate[8] of 148 ± 3 kcal/mol. This remarkable result will be further analyzed by us elsewhere in greater detail[39] by comparing our findings with experimental measurements. Suffice it to say here that the effect of complex formation with a competing base as occurring in the experiments[8] is seen from the present calculations to be one in which dehydrogenation effects are possibly introduced by the nonadiabatic contributions from the region of conical intersection that leads to the electron-transfer process with H formation that we shall discuss ion the next section. In other words, the possible increase in the density of states of the collision complex between the protonated adduct and the competing base molecule B, $[(O_3-H)^+-B]$, is likely to produce an increased lifetime of the latter whereby the crossing of the conical region can occur as the proton stretches out and therefore temporarily leads the "stretched" protonated adduct to an intermediate, H-bound species with B still present in the complex, followed by fast decay of the final protonated reference base:[39]

$$[(O_3-H)^+\cdots B] \rightarrow [O^+{}_3\cdots H-B] \rightarrow [O_3\cdots(H-B)^+] \quad (11)$$

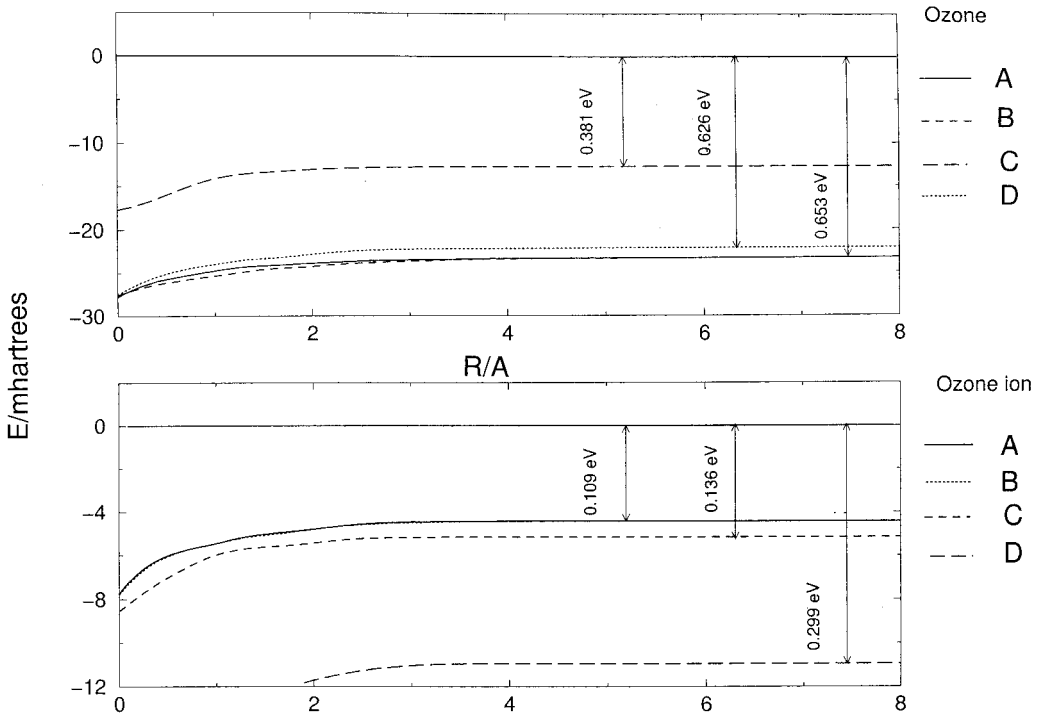

Figure 2. CP corrections for the asymptotic channels discussed in the main text. All calculations were done at the MCSCF-core level. The upper panel refers to the $O_3 + H^+$ asymptote and the lower panel to the $O_3^+ + H$ asymptote. Both molecules are kept at their asymptotic optimal geometries. All four protonated forms of Figure 1 are considered.

That the kinetics of protonation may not be the one-step mechanism usually assumed in the earlier calculations and experiments, but rather that the energetics of it may be guided instead by electronically nonadiabatic effects has also been suggested in rather general terms by a recent computational study.[40] It seems, however, that the role of such conical intersections is for the first time specifically suggested by the present calculations in what we shall show below to be the effects from marked, nonadiabatic regions within the nuclear phase space relevant to reaction transition complexes.[39]

5. Nonadiabatic Effects

When dealing with the basic interaction, in the gas phase, between a free proton and a molecule, several aspects of the possible outcomes are rooted in the features of the intermediate, metastable complex, often described as a highly excited state of the bound protonated adduct.[31] We have discussed in the previous sections the structural properties and the relative energetics of the lowest electronic state of the adducts and their geometries from the BO configurations of the bound electrons. We now wish to analyze a bit further the existence of different asymptotic states of the interacting partners, as briefly sketched in the Introduction.

From the experimental side, we know already that low-energy collisions between protons and neutral molecules lead to significant rotovibrational energy transfers[31,32] and that such excitations can occur within two different asymptotic exit channels of the dynamics, i.e., within the collisionally direct channel, where H^+ energy losses are measured, or the collision charge-transfer (CT) channel, where H is formed and the corresponding molecular ion also detected.[33,34]

Nonadiabatic transitions at potential curve crossings represent a very basic and significant mechanism for state or phase changes in a broad variety of dynamical processes.[35] Needless to say, there are several spectroscopic as well as collision processes in chemical reactions which are governed by nonadiabatic transitions at potential curve (or surface) crossings (or avoided crossings): even organic chemical reactions are often classified in terms of simpler curve crossing schemes.[36]

In the case of a polyatomic structure like $[O_3H]^+$ the initial step already appears computationally quite demanding. However, we shall show below that, at least within the selected cuts of the PES which are suggested by the four structures of Figure 1, it is possible to find the locations of the curve crossings and therefore the most likely paths for the occurrence of CT processes in the dynamics of proton collisions with ozone molecules. It is also well-known that the isolated O_3 molecule presents a $^1A_2-^1B_1$ conical intersection, which involves electronic states that are of singly excited character with respect to the ground state of ozone.[37] We shall show in a following study[38] that its protonated adduct also exhibits electronically induced conical intersections involving the ground electronic states and that the present avoided crossings are the one-dimensional signatures of such nonadiabatic effects.

To assess more quantitatively the relative energetics of the two final exit channels ($O_3 + H^+$ and $O_3^+ + H$), we started with the calculation of the O_3 ionization potential by optimizing the geometry of the O_3^+ ion to its ground electronic state. We therefore found for the adiabatic ionization potential a value of 11.07 eV from calculations without any ZPE or temperature corrections. The experimental[3] value is 12.53 eV, i.e., a discrepancy of 1.46 eV. This result therefore brings the asymptotic energy difference between channels, ΔE_∞, to be -2.533 eV, a value which, in comparison with the experimental value of -1.07 eV, is only qualitatively correct.

To improve such data, the results shown in Figure 2 report calculations for the four different cuts of the ground-state PES for the protonated adduct. The upper panel shows the CP calculations for the ozone molecule in the presence of the additional basis centered on the "dummy" H^+ nucleus over a broad range of relative distances. The total energy shown is that of the isolated neutral O_3. One sees that the CP corrections

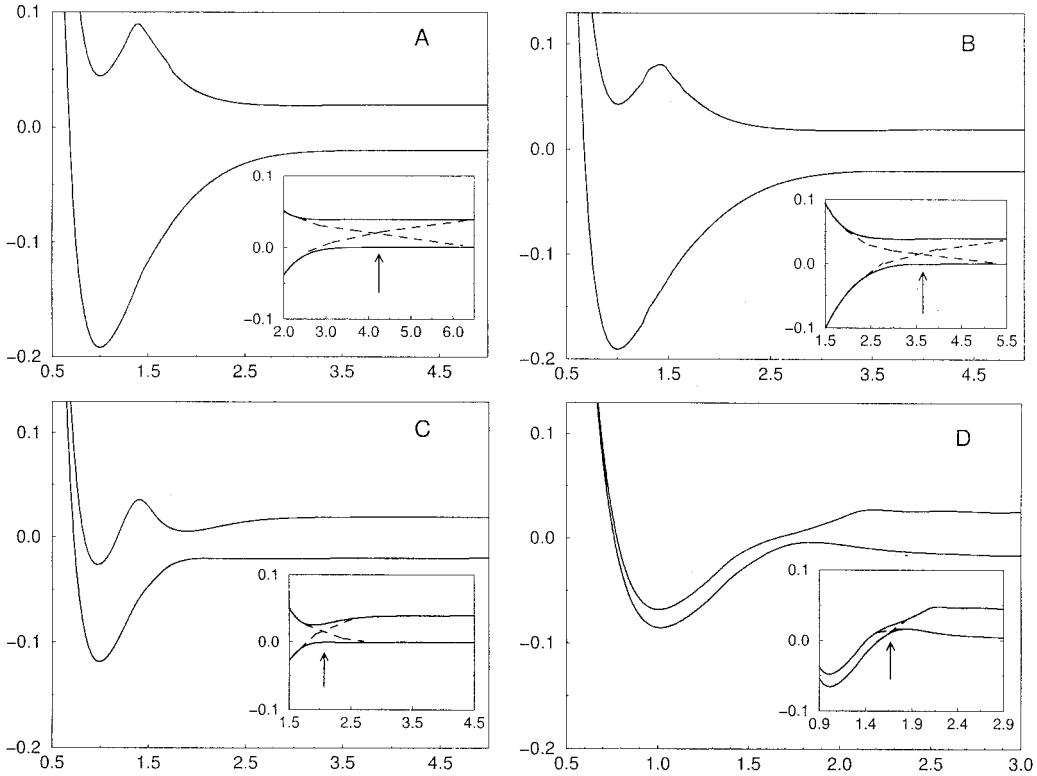

Figure 3. Behavior of the computed lowest two roots of the $(O_3H)^+$ system along the dissociative pathways for the two open-chain adducts, A and B (upper panels), and for C, D adducts (lower panels). The insets show enlarged views of all four avoided crossing regions. The dashed lines qualitatively indicate the diabatic curve behavior for each of the four crossings.

are fairly large, and comparable with each other, for three of the directions of approach but are much smaller for the case of the ring structure in C_{2v} geometry (C form in Figure 1). The lower panel shows CP-corrected calculations for the ozone ion and for the removal of a "dummy" H atom. Here again, only the total energy of the isolated molecular ion is shown. The CP corrections are now smaller as the H polarization effects are obviously reduced when compared with those from the receding proton: the largest correction now comes from the nonplanar ring structure (D form) while the A form shows now the smallest correction. From such findings, therefore, we can now get the corrected energy separation in the asymptotic region for the most stable A form as given by

$$\Delta E_{\infty}^{CP} = E_{O_3} - (E_{O_3^+} + E_H) = -1.98 \text{ eV} \qquad (12)$$

which is now closer to the experimental results (1.07 eV). It is worth remembering at this point that we are now required to use in full the ΔE^{CP} expression of eq 3 while eq 12 implies that we are disregarding the effect of the O_3^+ basis on the H total energy. Although we do not expect this correction to be very large (due to the small polarizability of H), it partly explains the discrepancy of about 0.88 eV.

To analyze more in detail the location of the crossings for each of the forms, we present on the upper side of Figure 3 the two lower roots for the paths of approach that follow the A and B configurations and we show them separated asymptotically by the experimental energy value of 1.07 eV. In the upper-left part we report the curve behavior for the open-chain A form, and in the upper-right part of the same figure we show the two curves for the B form. In the two insets we also show the two crossings on an enlarged energy scale. We should remind ourselves at this point that the BO curves reported there are neither adiabatic nor diabatic representations of the electronic interactions as a function of nuclear positions but direct results from the MCSCF-close calculations. Hence, due to the fact that the two states have the same symmetry, the two BO curves avoid each other and thefore two avoided crossings (shown by the dashed curves in the insets) can be found in the two open-chain protonated forms: they both occur at relatively large distances of the proton from the wing oxygen atom to which it is attached, hence the difficulty of seeing them with the naked eye.

The same type of calculation is shown on the lower part of Figure 3, where the two ring configurations of C_{2v} symmetry are shown: the planar C form (left side) and the nonplanar D form (right side). The calculations show that the asymptotic separations including the CP corrections are now larger (~2.2 eV) while the avoided crossings appear at shorter proton distances from the wing atom (at less than 2 Å in both cases).

As mentioned at the beginning of this section, when the electronic energy (BO calculations) of the separated $H^+ + M$ system lies above the energy level of the separated $H + M^+$ system, then the electronic state of the former asymptote in general correlates adiabatically with an excited electronic state of the adduct, $(MH)^{*+}$, while there is also likely to exist some special reaction path along which it is possible to smoothly pass from the electronic state which correlates asymptotically with $H^+ + M$ to the ground electronic state of the protonated adduct, $(MH)_0^+$. This special passage, which can continuously lead from the excited electronic state of the fragments to the ground electronic state of the combined system, can be called adiabatic in the sense of a smooth dependence of the electronic wave function on the nuclear coordinates along this path. On the other hand, it can also be called diabatic in the sense that it brings the system from an upper potential surface to a lower one.[35]

The results which we have shown in Figure 3 indicate the shape of just such a path which indeed brings smoothly the

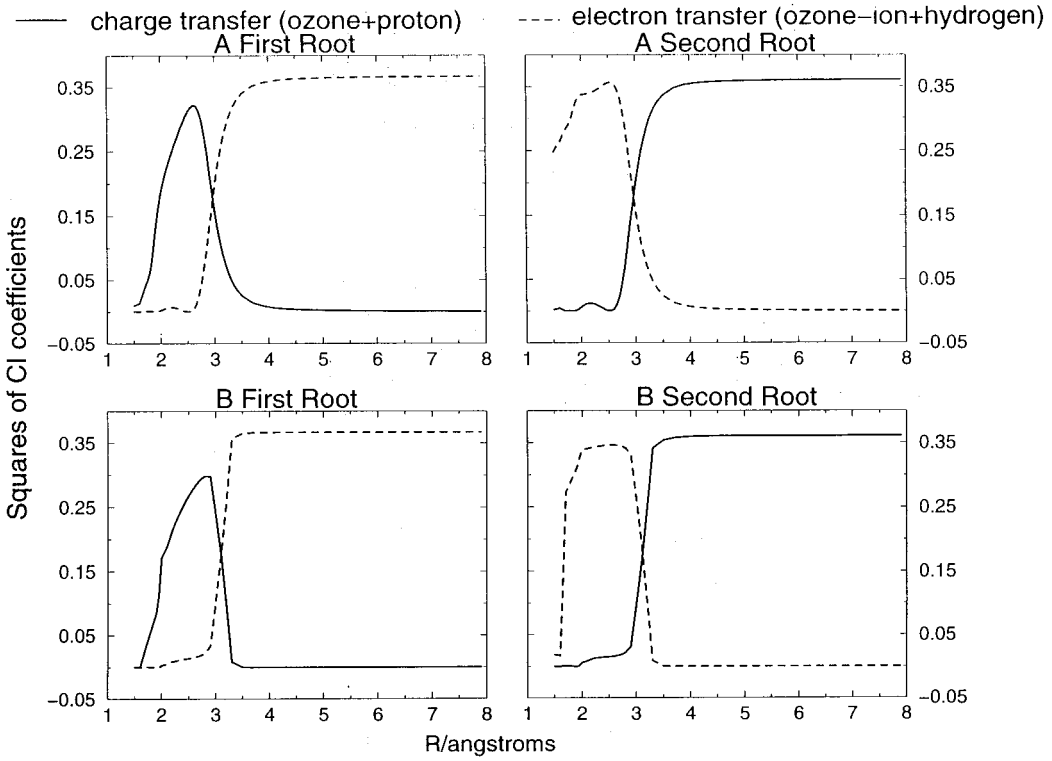

Figure 4. Behavior of the squares of the two largest CI coefficients for the lowest two roots of the open-chain structures. Top panels: coefficients for the A configurations. Lower panels: behavior for the B configurations. The "charge-transfer" root is marked by a solid line while the "electron-transfer" root is marked by a dashed line.

excited state that breaks up as $M^+ + H$ into the region of the lower well associated with all four forms of the protonated adduct. At the same time, such smooth passages recovered from the avoided crossings of the BO curves are also diabatic in the sense that they should "bring down" the system from the excited state into the lowest bound electronic state of the protonated adduct. This is most clearly demonstrated by the plots of the squares of the largest CI coefficients associated with the two lowest roots that we are considering here. Such plots are reported in Figure 4 for the two open-chain forms that were shown to be the most stable in the previous calculations, but similar plots can also be made for the ring structures C and D.

The left part of the figure contains the largest coefficients associated with the first roots from the MCSCF-close calculations for the A form (top) and the B form (bottom) in the region across the avoided crossings, while the corresponding second roots (excited states) are shown at the right-side part of the same figure. Furthermore, we show the coefficients that correspond to the charge-transfer process of eq 1 (i.e., when the positive charge is kept on the proton) with a solid line for both roots while the coefficients that lead to the ET process (and which asymptotically yield $O_3^+ + H$) are those given by the dashed lines. The following observations could be made:

(i) if we follow the coefficient behavior in the first root of the A form, we see that the removal of the H^+ partner dominates at the beginning, with little electron migration from the O_3 moiety since the weight of the electron-transfer root (dashed line) changes little at the outstart and is initially negligible. Up to about 2.5 Å the solid line reaches a maximum while the dotted line has not changed value; the H^+ is therefore moving away and the O_3 fragment is left "behind" in the adduct.

(ii) When the system is further separated and is getting closer to the crossing, however, the solid line rapidly drops and the dashed line increases: the electron is being transferred to the proton while the O_3 is becoming a positive ion. On the other hand, the second root for the same A form behaves in just the opposite way: the system starts as an electronically excited moiety $(O_3H)^{+*}$ where the polar bond is formed with contributions from ionic states of O_3 and a highly polarized H atom (see right upper panel in Figure 4). As the proton moves away from the complex, it leaves the electron "behind" while going toward the region of the crossing.

(iii) At the crossing point the two coefficients behave symmetrically in both roots: a stretched $(M-H)^+$ bond appears to be equally well described as either an (M^+-H) system with electron-transfer features or an $(M-H^+)$ system, with the electron being located on the molecular moiety.

(iv) Beyond the (avoided) crossing point one sees clearly from the coefficient behavior the nonadiabatic nature of the two "diabatic" curves: the first root, which comes from the ground state of the protonated moiety, is now dominated by the electron-transfer coefficient, which was absent in it around the equilibrium geometry, and moves out to the more energetic $M + H^+$ asymptotic products. On the other hand, the second root that was describing, at its equilibrium configuration, the $(MH)^{+*}$ excited moiety is now being dominated by the coefficient associated with the adduct moving along the CT channel that leads to the ionic molecule plus the H-atom configuration of the lower asymptotic channel.

A similar analysis of the B form also shown in the lower panels of Figure 4 follows essentially the same qualitative pattern as the previous example and exhibits even more abruptly the nonadiabatic feature of the avoided crossing: the sudden switching of the relative weights of the coefficients as the system goes through the region of the electronically nonadiabatic "electron jump".

The actual values of the energy gaps at the geometry of the minimum energy separations between BO curves are reported in Table 13.

TABLE 13: Energy Spacings between BO Cruves at the Relative Proton Approach of Minimum Energy Gap between the Two Lowest States

	A	B	C	D
R_{cross} (Å)	3.95	3.40	2.00	1.70
ΔE (meV)	1067.5	1052.2	723.7	0.27

6. General Conclusions

In the present work we have revisited the electronic structures of protonated ozone in the gas phase and analyzed their energy values and structural quality by making use of an extensively correlated calculation at the BO level. We have found that most stable forms are indeed given by "open-chain" planar structures, with the bound proton attached to one of the wing atoms. However, the calculation also confirms the presence of "ring" structures with the proton attached to the central oxygen atom and with a final configuration of C_{2v} symmetry, either planar or nonplanar.[12,13] The latter structures, as final forms, turn out to be less stable than the former ones but still provide two further intermediate complexes within the multidimensional PES of this four-atom protonated moiety.

The proton affinity of the system is known from mass spectrometric experiments,[8−10] and therefore we have attempted here, for the first time, to evaluate such a quantity from first principles using an extensively correlated electronic wave function and examining the contributions from several factors to the final gas-phase value. The results from our calculations show that the four final forms provide very different PA values. This therefore means that, depending on the microscopic kinetic mechanisms involved in the $(O_3H)^+$ formation, one could form with different probabilities each of the species found by the calculations and that our knowledge of this mechanism cannot tell us as yet which will be the dominant one. Purely energetics considerations on the *final* configurations would indicate the open-chain forms to be the more likely ones. However, the existence of nonadiabatic pathways amply shown by the present study also tells us that the strength of the coupling will also be an important contribution to the final kinetics.

We have, in fact, analyzed the electronic deformation of the system when the proton is removed from the stable adduct and found that two different asymptotic channels can be populated by gas-phase deprotonation. As expected, the system can undergo electron transfer under deprotonation and adiabatically follow the lower asymptotic channel where the molecular ion is formed ($O_3^+ + H$). On the other hand, it could also cross the nonadiabatic region between BO curves of C_s symmetry and evolve into the upper asymptotic channel where the positive charge of the moiety moves onto the receding proton and the neutral molecular partner is left behind. In the latter case, however, the nonadiabatic nature of the process is clearly seen by the behavior of the squares of the largest CI coefficients which show (see Figure 4) that the upper root, in the asymptotic region, is dominated by configurations which are negligible when describing the ground electronic state of the protonated adduct around its equilibrium geometry but appear instead when describing an electronically excited $(O_3H)^+$ system.

In conclusion, the present study suggests that the evaluation of the proton affinity in the gas phase from experimental and computational methods may proceed along different pathways in the sense that the gas-phase kinetics may not involve only the expected asymptotic partners from the inverse of eq 5 but might also proceed via nonadiabatic pathways which depend on the electronic structure of the partner molecule as surmised by the sequence of eq 11. That such discrepancies appear in ozone, and in other systems where nonadiabatic crossings have been found, will be the subject of our further, more detailed analysis of protonation kinetics.[39]

Acknowledgment. The financial support of the Italian National Research Council (CNR) of the Italian Ministry for Universities and Research (MURST) and of the Advanced Computing Consortium (CASPUR) is gratefully acknowledged. M.C. also thanks Residenza Universitaria ("Federazione Nazionale dei Cavalieri del Lavoro") for supporting a stay at the Chemistry Department of Warwick University in the summer−fall of 1997. The computational work was begun during that stay, and we therefore thank the British EPSRC for financial support.

References and Notes

(1) Lissi, E.; Heicklen, J. *J. Photochem.* **1972**, *1*, 39.
(2) Bates, D. R. *Physics of the Upper Atmosphere*; Academic: New York, 1960.
(3) Mathisen, K. B.; Gropen, O.; Skancke, P. N.; Wahlgren, U. *Acta Chem. Scand.* **1983**, *A37*, 817.
(4) Olah, G. A.; Yoneda, N.; Parker, D. G. *J. Am. Chem. Soc.* **1976**, *98*, 5261.
(5) Yoneda, N.; Olah, G. A. *J. Am. Chem. Soc.* **1977**, *99*, 3113.
(6) Nangia, P. A.; Benson, S. W. *J. Am. Chem. Soc.* **1980**, *102*, 3105.
(7) For example, see: Cipollini, R.; Crestoni, M. E.; Fornarini, S. *J. Am. Chem. Soc.* **1997**, *119*, 9499.
(8) Cacace, F.; Speranza, M. *Science* **1994**, *265*, 208.
(9) Speranza, M. *Inorg. Chem.* **1996**, *35*, 6140.
(10) Cacace, F.; Speranza, M. *Chem. Lett.* **1998**, 419.
(11) Mariey, L.; Lamotte, J.; Hoggan, P.; Lavalley, J. C.; Boulanine, K.; Tsyganenko, A. *Chem. Lett.* **1997**, 835.
(12) Kausch, M.; v. R.-Schleyer, P. J. *Comput. Chem.* **1980**, *1*, 94.
(13) Meredith, C.; Quelch, G. E.; Schaefer, H. F., III *J. Am. Chem. Soc.* **1991**, *113*, 1187.
(14) Toscano, M.; Russo, N.; Rubio, J. *J. Chem. Soc., Faraday Trans.* **1996**, *92*, 2681.
(15) Petsalakis, I. D.; Theodorakopulos, G.; Nicolaides, C. A. *J. Chem. Phys.* **1994**, *100*, 5870.
(16) Chamboud, G.; Rosmus, P.; Senent, M. L.; Palmieri, P. *Mol. Phys.* **1997**, *92*, 399.
(17) Hedström, M.; Morales, J. A.; Deumens, E.; Öhrn, Y. *Chem. Phys. Lett.* **1997**, *279*, 241.
(18) Scuseria, G. A.; Lee, T. J.; Scheiner, A. C.; Schaefer, H. F. *J. Chem. Phys.* **1989**, *90*, 5635.
(19) Osamura, Y.; Yamaguchi, Y.; Saxe, P.; Vincent, M. A.; Gaw, J. F.; Schaefer, H. F. *Chem. Phys.* **1982**, *72*, 131.
(20) Werner, H. J.; Knowles, P. J. *J. Chem. Phys.* **1988**, *89*, 5803.
(21) Werner, H. J.; Knowles, P. J. *Chem. Phys. Lett.* **1988**, *145*, 514. Werner, H. J. *Adv. Chem. Phys.* **1987**, *59*, 1.
(22) Werner, H. J.; Knowles, P. J. *J. Chem. Phys.* **1985**, *82*, 5053. Roos, B. O. *Adv. Chem. Phys.* **1987**, *69*, 399.
(23) Lucchese, R. R.; Schaefer, H. F. *J. Chem. Phys.* **1997**, *67*, 848.
(24) Banichevich, A.; Peyerimhoff, S. D. *Chem. Phys.* **1993**, *174*, 93.
(25) For example, see: van Duijneveldt, F. B.; van Duijneveldt-van de Rijdt, G. C. M.; van Lenthe, J. H. *Chem. Rev.* **1994**, *94*, 1873.
(26) Chalasinski, G.; Gutowski, M. *Chem. Rev.* **1988**, *88*, 943.
(27) Fowler, P. W.; Buckingham, A. D. *Mol. Phys.* **1983**, *50*, 1349.
(28) Boys, S. F.; Bernardi, F. *Mol. Phys.* **1970**, *19*, 553.
(29) Lin, B.; McLean, A. D. *J. Chem. Phys.* **1973**, *59*, 4557.
(30) Benson, S. W. *Thermochemical Kinetics*; John Wiley and Sons: New York, 1976.
(31) Gierz, U.; Noll, M.; Toennies, J. P. *J. Chem. Phys.* **1985**, *83*, 2259.
(32) Noll, M.; Toennies, J. P. *J. Chem. Phys.* **1986**, *85*, 3313.
(33) Gianturco, F. A.; Palma, A.; Semprini, E.; Stefani, F.; Baer, M. *Phys. Rev. A* **1990**, *42*, 3926.
(34) Baer, M.; Niedner-Schatterburg, G.; Toennies, J. P. *J. Chem. Phys.* **1989**, *91*, 4969.
(35) Nikitin, E. A.; Umanski, S. Ya. *Theory of Slow Atomic Collisions*; Springer Verlag: Berlin, 1984.
(36) Shaik, S.; Hiberty, P. C. In *Theoretical Models of Chemical Bonding*; Marsic, Z. B., Ed.; Springer Verlag: Berlin, 1991.
(37) Domcke, W.; Woywod, C. *Chem. Phys. Lett.* **1993**, *216*, 362.
(38) Ceotto, M.; Gianturco, F. A. Submitted to *J. Chem. Phys.*
(39) Ceotto, M.; Gianturco, F. A.; Speranza, M. Manuscript in preparation, 1999.
(40) Contreras, R.; Safant, V. S.; Andrês, J.; Pêrez, P.; Aizman, A.; Tapia, O. *Theor. Chem. Acc.* **1998**, *99*, 60.